RSC Advances

ROYAL SOCIETY OF CHEMISTRY

www.rsc.org/advances

RSC Advances

MANUSCRIPT ID: RA-ART-04-2015-007613

A turn off and reversible fluorescence probe (HNAPP) for Zn(II) ion towards inorganic phosphate ions (H_2P and HP) at physiological pH†

Amar Hens*

Abstract

A simple and low cost new schiff base compound (HNAPP) of 2-hydroxynaphthaldehyde and 2-amino-3-phenyl-1-propanol was synthesized and characterized by ^{1}H NMR and mass spectroscopic technique. The optimized structure of the probe in different polarity solvent and potential energy scan revels that the probe stable as an enol tautomer in polar solvent while in less polar solvent keto tautomer is more prominent. In dichloromethane the keto tautomeric form of the probe undergoes an excited state intramolecular proton transfer, ESIPT, stable as an enol structure, reveals unusual relaxation routes after electronic excitation. The results accompanied by TDDFT calculations are used to construct the diagram of relaxation routes of an excited HNAPP molecule. The probe exhibited high selectivity and sensitivity turn-on fluorescence emitter towards Zn^{2+} over other common metal ions in a physiological pH window with a 2:1 binding mode. The association constant, K_{assoc} observed at 5.2 x 10^{4} M^{-1}. The fluorescence decay constant (s) values were determined from time resolved fluorescence study. The addition of inorganic phosphate ions has been quenched the fluorescence intensity of the complex with different pH, making receptor HNAPP a reversible chemosensor act as a pH modulator. On the basis of these observations, I developed a unique molecular system capable of performing logic function such as INHIBIT, by simply varying the level of various ionic inputs in a systematic manner.

Introduction

The development of chemo sensors that have the capability to selectively recognize and sense metal ions is one of the most challenging fields in chemistry.[1] Amongst the available detection methods, chemo sensors which are based on ion-induced fluorescence changes have become predominantly attractive in terms of sensitivity, selectivity, response time, simplicity, high degree of specificity and low detection limit.[2] Zinc is the second most abundant transition metal in human body after iron and plays important roles in various pathological processes.[3] So far, search for reagents which can efficiently act as fluorescence probes for Zn(II) at physiological pH has been an active area of research.[4]

Zn(II) ion is spectroscopically as well as magnetically silent due to its $3d^{10}$ electronic configuration. However it can modulate the ligand luminescence properties by means of chelation enhanced fluorescence's (CHEF).[5] The generated CHEF effect is regulated by photoinduced electron transfer (PET) mechanism. In this context the Schiff base complex of Zn(II) ion are particularly interesting due to their potential photochromic applications.[6]

In addition, it is still a challenge to develop chemo sensors that can discriminate Zn^{2+} from Cd^{2+},[7] because cadmium and zinc are in the same group of the periodic table and have similar properties, which usually cause similar spectral changes after interacting with chemo sensors. In these sense, the design and synthesis of fluorescent selective Zn^{2+} chemo sensors are of great interest. Despite some commercial fluorescent probes for Zn^{2+},[8] the design of facile, easy to synthesize, nontoxic Zn^{2+}-selective probes is still a challenging task, and there is a need for the design and synthesis of such chemo sensors, which are small molecules and highly sensitive for real-time detection in biological systems at physiological pH. My synthesized probe HNAPP selectively detect Zn^{2+} ion over the presence of other cations specially Cd^{2+} at physiological pH window.

Phosphates are one of those target anions, as they play significant roles in many biological processes, such as cellular ATP hydrolysis, DNA and RNA polymerizations, and many enzymatic reactions.[9] Recently, the detection of inorganic phosphate ions such as mono hydrogen phosphate (HP) and di-hydrogen phosphate (H_2P) has become an important issue for cancer research and for rheumatological disorder that arises due to the accumulation of crystals of calcium pyrophosphate dihydrate in the connective tissues.[10] Thus, the specific recognition and sensing of inorganic phosphate under physiological conditions is of immense significance.

In this report, I show that the aminopropanol–naphthalene based ligand, HNAPP, when forming a complex with Zn^{2+} is highly fluorescent. This [Zn-$NAPP_2$] complex has been utilized as a receptor for both HP and H_2P in mixed aqueous medium by a metal displacement approach which results in the quenching of fluorescence. Some aspects of these unanticipated findings were streamlined by DFT and TDDFT calculations.

Experimental section

Materials

The transition metal salts used in the present investigation are as follows: $Zn(ClO_4)_2.6H_2O$, $Cr(ClO_4)_3.6H_2O$, $Cu(ClO_4)_2.6H_2O$, $Mn(ClO_4)_2.6H_2O$, $Ni(ClO_4)_2.6H_2O$, $Co(ClO_4)_2.6H_2O$ and $Cd(ClO_4)_2.6H_2O$. The metal salts were procured locally and were used as received. Perchlorate salts were preferred because of the low coordinating ability of the anionic counterpart. Tetrabutylammonium (TBA) salts of the respective anions ([A] = F^-, Cl^-, Br^-, I^-, OAc^-, $H_2PO_4^-$ (H_2P), HPO_4^{2-} (HP), $P_2O_7^{4-}$ (PPi) and CN^- "A" stands for anion) sodium salt of ATP, ADP and AMP were used as received from Sigma-Aldrich, USA. MES (2-(N-morpholino)ethanesulfonic acid, HEPES 4-(2-hydroxyethyl)piperazine-1-ethanesulfonic acid, and TRIS (tris(hydroxymethyl) aminomethane, potassium chloride and hydrochloric acid were purchased from Cyno-chem, India. All other solvents and reagents such as dichloromethane (DCM), methanol (MeOH), acetonitrile (CH_3CN) and dimethylformamide (DMF) were of spectroscopic grade (Spectrochem, India) and used after proper distillation. The solvent was found free from impurities and appeared transparent in the spectral region of interest. The purity was also verified by recording the emission spectra in the studied spectral region. $CDCl_3$ for NMR experiments were used as received from Sigma-Aldrich, USA.

Caution! *Perchlorate salts are highly explosive, and should be handled with care and in small amounts.*

Physical Measurements

UV–Vis spectra were recorded on a Perkin–Elmer LAMBDA 25 spectrophotometer. Electrospray ionization mass spectrometry (ESI-MS) measurements were done on a Micromass Qtof YA 263 mass spectrometer. The molar conductivity was determined using Systronics Conductivity Meter 304 in acetonitrile solution at room temperature. Elemental analyses (C, H, N) were performed on Perkin–Elmer 2400 series II analyzer. The emission data was collected on

a Perkin-Elmer LS 55 fluorescence spectrometer. All pH measurements were made with a pH-10C digital pH meter. Quantum yields of the ligand and complex were determined in freeze-pump-thaw-degassed solutions of the ligand and complex by a relative method using quinine sulfate in the same solvent as the standard.[11] and calculated using eq 1,[12a] where Φ_r and Φ_{std} are the quantum yields of unknown and standard samples [$\Phi_{std} = 0.54$ (at 298 K) in methanol at λ_{ex}= 350 nm], A_r and A_{std} (<0.1) are the solution absorbance at the excitation wavelength (λ_{ex}), I_r and I_{std} are the integrated emission intensities, and η_r and η_{std} are the refractive indices of the solvent.

$$\Phi_r = \Phi_{std} \frac{A_{std}}{A_r} \frac{I_r}{I_{std}} \frac{\eta_r^2}{\eta_{std}^2} \qquad (1)$$

The fluorescence decay data were collected on a Hamamatsu MCP photomultiplier (R3809) and were analyzed by using IBH DAS6 software. The observed decays of the complex fitted well with a bi exponential function as in eq 2 and 3, where τ_1 and τ_2 are the fluorescence life time and α is the pre-exponential factor. For the fits, reduced χ^2 values are around one, and the distribution of weighted residuals was random among the data channels. τ_f is the mean fluorescence life time (meaning of the symbol are usual).[12b] All absorption and emission spectral measurements were performed with proper background corrections and with freshly prepared solutions only.

$$I(t) = [\alpha_1 \exp(-t/\tau_1) - \alpha_2 \exp(-t/\tau_2)] \qquad (2)$$

$$\tau_f = \alpha_1\tau_1 + \alpha_2\tau_2 \qquad (3)$$

Computational details

I also calculated and analyzed the singlet ground state natural transition orbitals (NTOs) derived from TDDFT results and compared them with the ground state molecular orbitals (MOs) obtained from DFT calculations. The computational modeling of the NMR parameter is also of abiding interest, and such DFT calculations have emerged as a promising approach for the prediction of nuclear shielding and coupling constants of NMR active nuclei.[13] Thus, I computed the proton NMR chemical shifts and also the ^{1}H-^{1}H spin-spin coupling constant using the gauge-independent atomic orbital (GIAO)-DFT method, which was aimed at providing the definitive characterization of the probe. The geometrical structure of the ligand (HNAPP) in their singlet ground (S_0) and excited state (S_1) were optimized by the DFT[14] and time-dependent DFT

(TDDFT)[15] method with B3LYP exchange correlation functional[16] approach associated with the conductor-like polarizable continuum model (CPCM).[17] The geometry of the probe was fully optimized in at different polarity solvent without any symmetry constraints. The vibrational frequency calculation was also performed for ligand to ensure that the optimized geometries represent the local minima and there are only positive eigen values. On the basis of the optimized ground (S_0) geometry of the ligand, the absorption properties in DCM media were calculated by TDDFT approach. To calculate the stability of the keto tautomeric form over the enol form for the ligand in ground S_0 state I performed the potential energy scan according to the "distinguished coordinate approach"[18] i.e. by specifying a reaction coordinate (in the present case it is the coordinate for translocation of the proton from N_{donor} to $O_{acceptor}$, i.e. elongation of the N_{donor} –H bond axis) along which energy change is observed. For the ground S_1 state all of the other degrees of freedom are relaxed without imposing any symmetry constraints. For H atoms, I used 6-31(g) basis set and for C, N and O atoms 6–31+g as basis set for the optimization of the ground state geometries. The calculated electronic density plots for frontier molecular orbitals were prepared by using the GaussView 5.0 software. All the calculations were performed with the Gaussian 09W software package.[19] GaussSum 2.1 program[20] was used to calculate the molecular orbital contributions from groups or atoms.

In addition, the ^{1}H NMR properties of the HNAPP were calculated with the magnetic field perturbation method with the GIAO algorithm[21] with the NMR = spin-spin keyword incorporated in the Gaussian 09W program. The relative chemical shift of a given nucleus X in the molecule was defined as δ_X^{calc} [ppm] = $\sigma_X^{ref} - \sigma_X^{calc}$ where TMS was used as a reference molecule optimized at the same level of theory.[22] In order to account for the solvent effect, I used the integral equation-formalism polarizable continuum model (IEFPCM) method.[23a.b]

Synthesis of Probe (HNAPP)

To a methanolic solution (20 mL) of 2-hydroxynaphthaldehyde (345 mg, 2 mmol), 2-amino-3-phenyl-1-propanol (305 mg, 2 mmol) was refluxed in water bath for 2 hours. After cooling to room temperature, the solvent was removed under reduced pressure. The crude mass was then subjected to column chromatography on a silica gel column (60-120 mesh). A light yellow band was eluted using 5% ethyl acetate in hexane solution. A yellow colored solid was obtained after removal of solvent under reduced pressure to afford the desired ligand. Yield: 433

mg (71%). Elemental Anal. Calcd. for $C_{20}H_{19}NO_2$: C, 78.66; H, 6.27; N, 4.59. Found: C, 78.30; H, 6.25; N, 4.82. ^{1}H NMR {300 MHz, CD_3Cl, δ (ppm), *J* (Hz)}: 14.20-14.15 (ArOH, bs), 8.41 (N=CH_2, s), 7.52 (1H, d, *J*=8.3 Hz), 7.32-7.20 (8H, m, ArH), 7.11-7.06 (1H, m, ArH), 6.68 (1H, d, *J*=9.2 Hz), 4.63-4.61 (AlOH, bs), 3.93-3.90 (PHCH_2, m), 3.76-3.70 (CH_2OH, m), 3.06-2.88 (1H, m). ESI-MS (CH_3CN): *m/z* Calcd. 306.1416, Found: 306.1296 (100%). $(HNAPP + H)^+$.

Synthesis of Complex

[Zn-$NAPP_2$], **1.** An aqueous solution of $Zn(ClO_4).6H_2O$ (0.037 g, 0.1 mM) was added to a methanolic solution of HNAPP (0.061 g, 0.2 mM) and the reaction mixture was warmed in water bath with care. A dilute methanolic solution of Et_3N (0.040 g, 0.40 mM) was then added to the reaction mixture to maintain at a pH of 7-8; then refluxed for 2 hours with afforded air and was allowed to cool to room temperature. The reaction mixture was then filtered, and the volume of solvent was reduced via rotary evaporator to obtain colorless residue. The residue was filtered and washed by methanol and was then dried in vacuum. The solution was kept for slow evaporation which yielded colorless crude product in good amount. Yield: 47 mg (70%). Elemental Anal. Calcd. for $C_{40}H_{34}N_2O_4Zn$: C, 71.48; H, 5.10; N, 4.17. Found: C, 71.34; H, 5.17; N, 4.15. ^{1}H NMR {300 MHz, CD_3CN, δ (ppm), *J* (Hz)}: 8.69 (N=CH_2, s), 7.72 (1H, d, *J*=6 Hz ArH), 7.46-7.13 (9H, m, ArH), 6.69 (1H, d, *J*=10 Hz ArH) 3.65 (2H, PHCH_2), 3.47 (2H, CH_2OH) and 3.06-2.88 (1H, m) ESI-MS (CH_3CN): *m/z* Calcd. 673.2045, Found: 673.2388 (100%) $(1 + 3H)^+$. Molar conductance, Λ_M: (CH_3CN) 265 Ω^{-1} cm^2 mol^{-1}.

Results and discussion

Synthesis

The tridentate *N,O,O* ligand (HNAPP) was made to react with $Zn(ClO_4)_2 \cdot 6H_2O$ in a ratio of 2:1 in methanol at room temperature in air to produce complexes of composition [Zn-$NAPP_2$] **1** in excellent yields. NAPP is the deprotonated form of the ligand. A schematic representation for the synthesis of ligand and complex is given in Scheme 1.

Conductance measurement and Mass spectra

The molar conductivity of the complex was determined in acetonitrile solution at room temperature. The value of the molar conductivity was 265 S cm^2 mol^{-1} which corresponded to a

2:1 type electrolyte. The ligand and complex were diluted with acetonitrile for mass spectrometry. Mass spectral analysis in the positive ion mode showed a major peak at *m*/*z* (%) = 306.1296 (100), which is assigned to the mono cationic protonated ligand $[HNAPP + H]^+$. The complex a major spectra appeared at *m*/*z* (%) = 673.2388 (100), allocated for the bischelate monomeric form of $[Zn\text{-}NAPP_2+3H]^+$. The mass spectrums were given in ESI Figs. S1 and S2†.

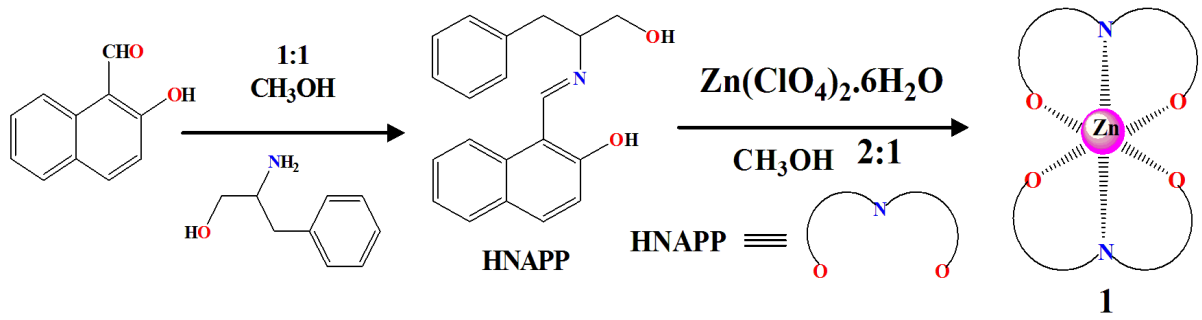

Scheme 1 Synthesis of receptor and complex.

NMR spectra

The ligand and complex are diamagnetic and display well resolved ^{1}H NMR spectra in CD_3Cl solution. HNAPP shows two distinguishable broad peaks at 14.20 and 4.6 ppm (Fig. 1). The peak appeared at deshielding region is assigned for phenolic proton whereas shielding region peak accounts for alcoholic proton respectively. These both peaks are completely disappeared during complex formation (ESI Fig. S3†). The singlet sharp peak near at 8.41 ppm is due to azo methine proton of the ligand under goes down field region around at 8.69 ppm during complexation. The aromatic protons span are 7.11-7.06 ppm and 7.46-7.13 ppm for the ligand and complex respectively. It was observed that due to complex formation almost all the arometic protons are suffer in deshielding regions as well as larger splitting of arometic span is attributed for symmetry lost during complexation. The methylene proton showed at 3.92 ppm and 3.73 ppm for ligand. The correlation between the experimental and calculated ^{1}H NMR chemical shift of HNAPP is shown in inset of Fig. 1 as a representative case.

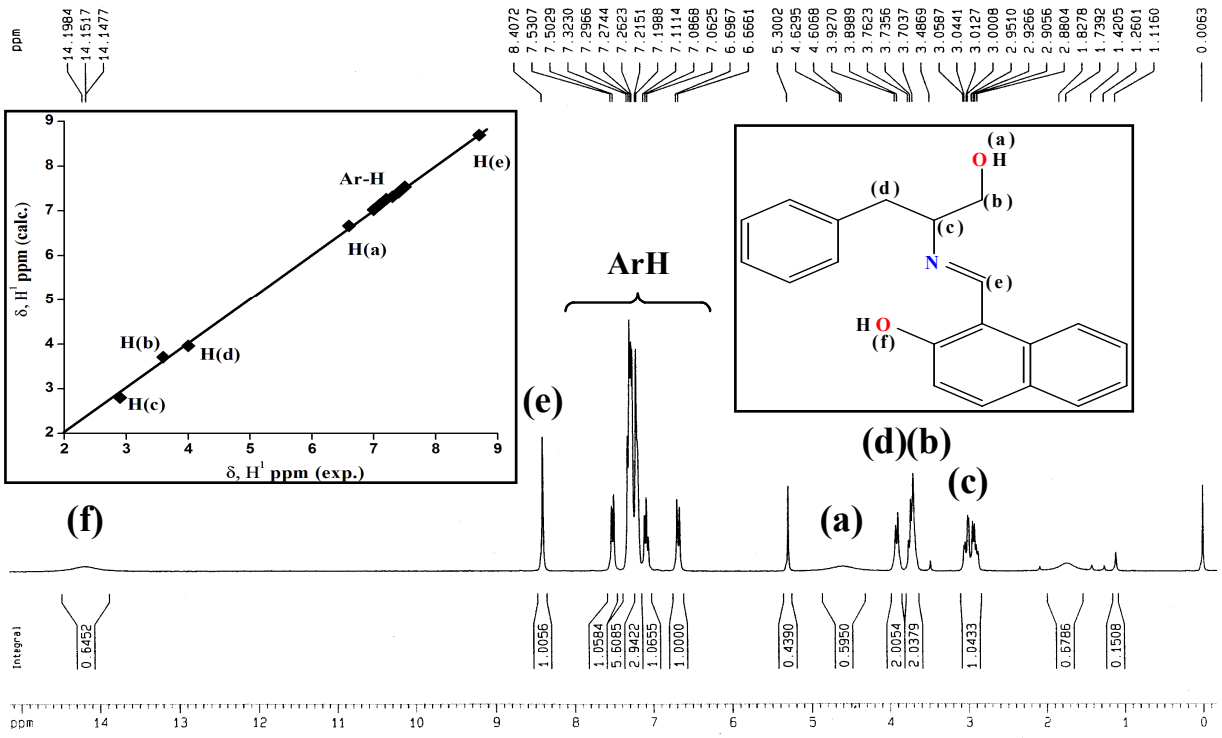

Fig. 1 The ^{1}H NMR spectra of HNAPP with their spectral nature of both aromatic and aliphatic region; In inset: Linear correlation between the experimental and calculated ^{1}H NMR chemical shifts of HANPP in aliphatic and aromatic regions.

Ligand photophysical study

The UV-Vis absorption spectrum of the probe shows two well resolved peaks near around 400 and 300 nm in solvent of different polarity at room temperature. The peak around 400 nm split into two distinguishable humps. As shown in Fig. 2, HNAPP shows low energy band at approximately 400 nm which is attributed to the n–π^* electronic transition whereas the prominent high energy band around at 300 is due to the π–π^* electronic transition. Z. Li. et al., showed a ground state keto-enol tautomerisation by varying the percentage of water in ethanolic medium.[23c] Herein, I also established similar type of ground state equilibrium by using different polarity solvents. The natures of electronic transitions are well established from TDDFT studies on the ground state optimized structure (S_0) of keto and enol forms of the ligand respectively. The theoretical UV-Vis spectra of enol and keto forms are given in electronic supplementary

materials (Figs. S4 and S5†). The spectra obtained from keto form is shows peak at 315 nm with higher oscillating strength while for the enol form the peak appears at 405 nm (Table S1†). The absorbance intensity of transitions of low energy band corresponding to electronic transitions, n–π^* of enol form and high energy band corresponding to electronic transitions π–π^* of keto form of HNAPP was show a dependence on the nature of the solvent polarity. The dynamic keto-enol equilibrium preferred to enol tautomeric form in more polar solvent whereas keto form is predominant in less polar solvent. The selectively O–H, C–O, N–H and N–C bond distance of ground state optimized structure (S_0) of the probe in different polarity solvent clearly indicates that polarity of the solvent controlled the equilibrium constant of keto-enol tautomerization (Table 1). The ground state optimized structure in DCM, MeOH and DMF are given in ESI Fig. S6†.

Table 1 Optimized structural parameter of HNAPP in different polarity solvent.

Solvent	H–O Å)	C–O (Å)	N–H (Å)	N–C (Å)
DCM	1.96	1.27	1.03	1.33
MeOH	1.06	1.36	1.60	1.29
DMF	0.96	1.37	1.80	1.29

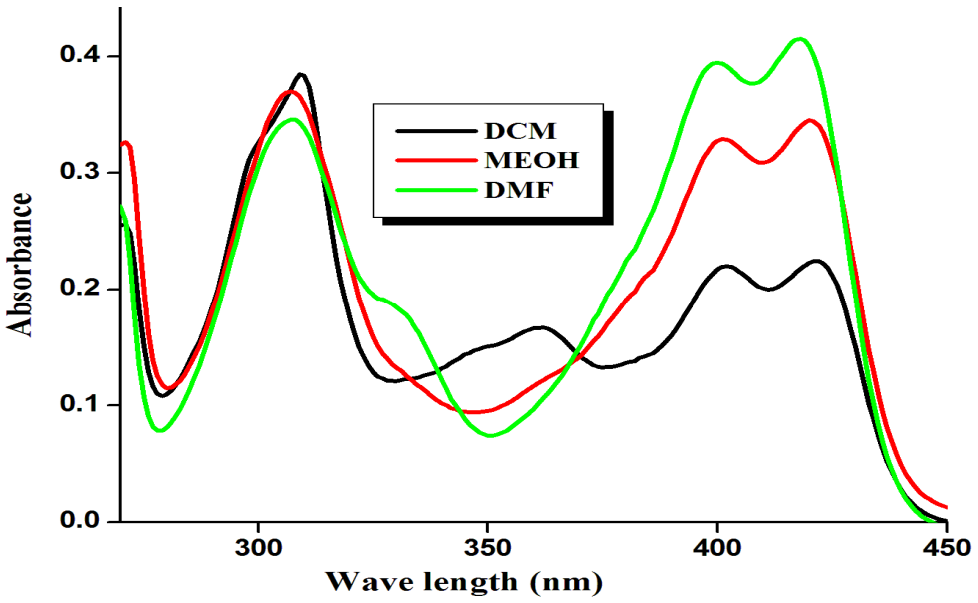

Fig. 2 The absorbance spectra of HNAPP (1 x 10^{-5} M) in different solvents at room temperature.

The absorption energies associated with their oscillator strengths, the main configurations and their assignments calculated using TDDFT method using the S_0 geometry for HNAPP is discussed here and the related data are given in Table 2. In case of ground state (S_0) the electron density at HOMO and HOMO-1 are delocalized over the naphthalene and phenyl moieties respectively, while in case of LUMO it originates from the contribution of both naphthalene (61%) and azo methine (35%) moieties. The calculated absorption bands located at 418 and 328 nm are in good agreement with the experimental result. The lower energy band can be assigned to the $S_0 \rightarrow S_1$ with distribution of electron density of non bonded oxygen to anti bonding orbital of azo methine moiety (n–π^*) whereas the higher energy band arises due to $S_0 \rightarrow S_3$, transitions, with allocation of electron density of π orbital of phenyl ring to π^* orbital of naphthalene and azo methine moieties. Frontier molecular orbitals involved in the UV-Vis absorption for HNAPP were given in Fig. 3.

Table 2 Selected Parameters for the Vertical Excitation (UV-Vis Absorptions) and the Emission of HNAPP; Electronic Excitation Energies (eV) and Oscillator Strengths (*f*), Configurations of the Low-Lying Excited States of HNAPP; Calculation of the S_0–S_1 Energy Gaps Based on Optimized Ground-State Geometries (UV-Vis Absoption) and the Optimized Excited-State Geometries (Fluorescence) (DCM used as solvent)

Process	Electronic Transitions	Composition	Excitation energy	Oscillator strength (*f*)	CI	λ_{exp} (nm)
Absorption	$S_0 \rightarrow S_1$	HOMO → LUMO	2.9848 eV (418 nm)	0.6669	0.70493	400
	$S_0 \rightarrow S_3$	HOMO – 1 → LUMO HOMO – 3 → LUMO	3.7698 eV (328 nm)	0.3798	0.64327 0.25444	300
Emission	$S_1 \rightarrow S_0$	HOMO → LUMO	2.4653 eV (503 nm)	0.1381	0.69282	492

The fluorescence spectral measurement for receptor in the absence of Zn^{2+} ions was carried out in DCM at room temperature (ESI Fig. S6†). Free HNAPP upon excitation at 400 nm have shown emission band at 492 nm with Stokes shift 92 nm with quantum yields (Φ_F) around

0.051. The ground S_0 state of HNAPP in DCM is Keto form (Fig. S4c†) whereas the S_1 state is enol form (Fig. S4d†).

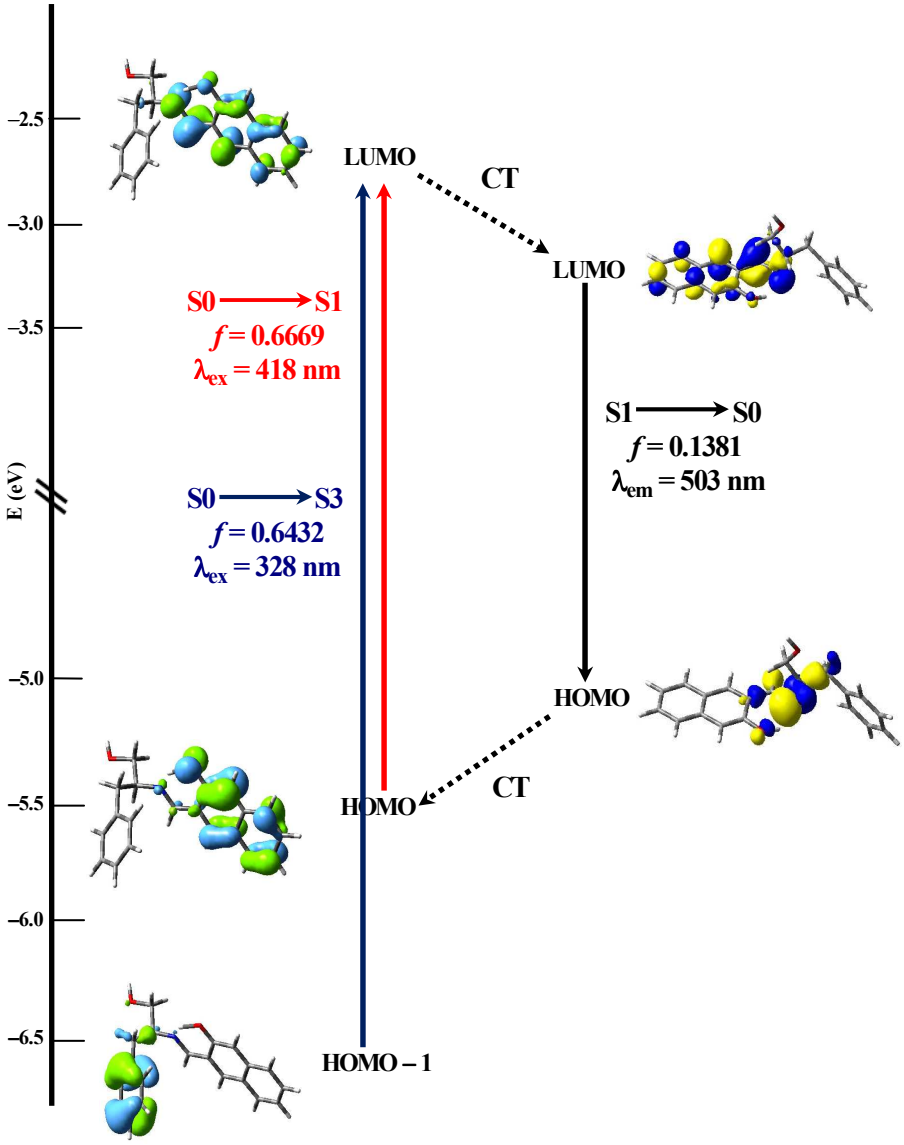

Fig. 3 Frontier molecular orbitals involved in the UV-Vis absorption and emission of HNAPP. CT stands for conformation transformation. Excitation and radiative decay process are marked as solid lines and the non-radiative processes are marked by dotted lines.

It was clear from S_1 state optimized structure in DCM attributed that the fluorescence excitation spectrum that there were two routes of creation of the excited enol tautomer: the tautomerization via the excited keto form (the ESIPT route), and the direct excitation of the keto tautomer. In

order to study the emission property, the potential energy scan of HNAPP was performed which reveals that the two tautomeric forms are exist at ground state in which enol form is more stable than keto tautomeric form over an amount of energy (ΔG) 0.1338 $eVmol^{-1}$. The transition energy required ($\Delta G^{\#}$) for this keto-enol tautomerization is 0.1679 $eVmol^{-1}$ (Fig. 4a).

The energy gap between the S_0 and S_1 state, calculated with the optimized S_1 state geometry, is the fluorescence emission wavelength. This geometry relaxation upon photo excitation imparts remarkable effect on the energy level of the molecular orbitals. In case of HNAPP the LUMO is stabilized by 0.75 eV at the S_1 state geometry compared to that at S_0 state geometry while the HOMO is destabilized by 0.36 eV for S_1 state geometry compared to that at S_0 state geometry. As a result, the energy difference between the HOMO and LUMO is greatly decreased at the S_1 state compared to that at S_0 state geometry and this geometry relaxation is the main origin of large Stoke shift. The fluorescence wavelength was calculated as 503 nm (in DCM) which is in very good agreement with the experimental value of 492 nm (Fig. 3).

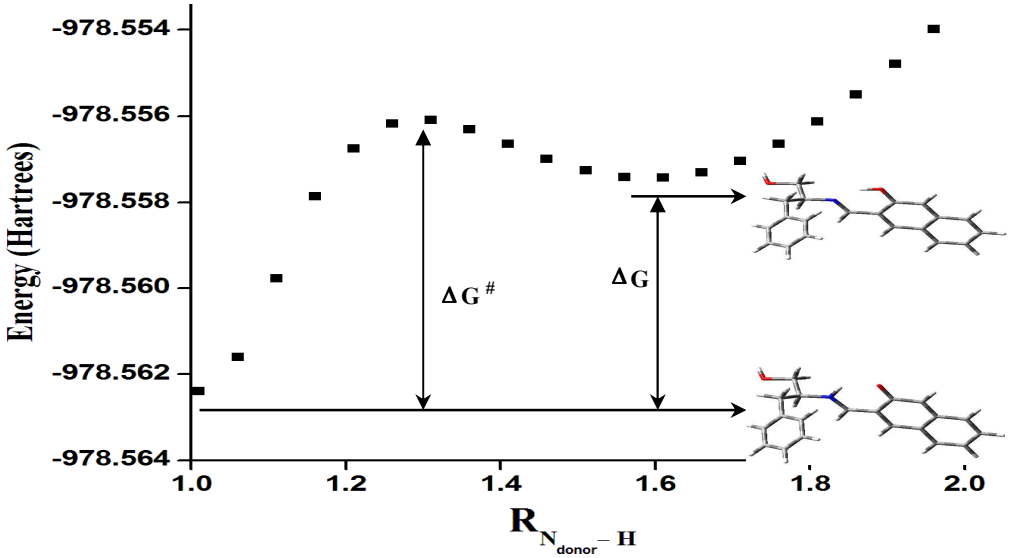

Fig. 4a potential energy curves for HNAPP calculated at DFT/B3LYP level.

UV-Vis Titration of HL with Zn(II)

As shown in Fig. 4b described a representative UV-Vis titration curve of HNAPP with various concentration of Zn^{2+} ions. The probe showed two humps around 400 nm. It has been observed that the absorbance intensity of both the hump appeared around 400 nm decreases with increasing concentration of Zn^{2+} ion with some blue shift (~10 nm). The similar trend also

observed at 320 nm whereas the reversed trend appeared at shorter wavelength at 250 nm and the yellow color of the ligand finally becomes colorless, which can be seen by the naked eye. The whole process has been passing through four distinguishable isosbestic points at 240, 292, 348 and 384 nm respectively. It is to be noted that there is no changes of absorption intensity both at 250 nm, 320 nm and 400 nm after the addition of excess of ~1.0 equivalent of Zn^{2+} ion with respect to ~2.0 equivalent of HNAPP. Jobs plot of maximum absorption intensity shows [M]/([M]+[L]) value is 0.321, which indicating 2:1 complex formation of HNAPP with Zn^{2+} (Inset of the Fig. 4b).

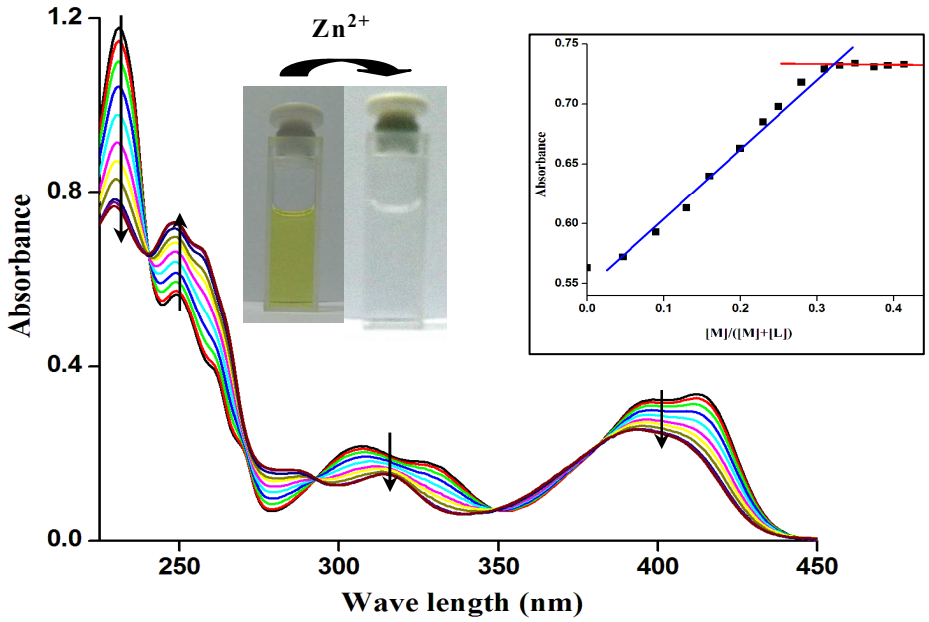

Fig. 4b Spectrophotometric titrations of HNAPP (10 μM) with various numbers of equivalent of Zn^{2+} at room temperature ($[Zn^{2+}]$ = (0–7 x 10^{-6} M). Insets: the corresponding titration profiles confirm the 2:1 (HNAPP: Zn^{2+}) binding stoichiometry (The absorbance values taken the corresponding wavelength at 250 nm).

Fluorogenic Zn(II) sensing

To determine the practical applications, the fluorescence response behavior of the probe were examined upon treatment with various metal ions in 10 mM HEPES aqueous buffer–CH_3OH (3 : 2, v/v). Fig. 5 shows the bar diagram of fluorescence intensity of HNAPP in the presence of different metal ions. Only Zn^{2+} resulted in a pronounced fluorescence enhancement,

whereas other transition metal ions including Cu^{2+}, Ni^{2+}, Co^{2+}, Mn^{2+}, Cd^{2+} and Cr^{3+} did not induce fluorescence as there is a probability of an electron and energy transfer between the metal ion and probe. When the experiment was carried out with ubiquitous intracellular metal ions such as K^+, Na^+ and Ca^{2+}, which exist at very high concentrations inside the cell, no significant fluorescence was observed, even at concentrations that were 10-fold higher than Zn^{2+} ion concentration (Fig. 5, blue bar). Metal-ion selectivity was also examined to probe if HNAPP could be used as a selective probe for Zn^{2+} in the presence of other competitive cations found in biological systems. Emission spectra were measured for a 2:1 mixture of HNAPP and Zn^{2+} in the presence of other metal ions. The prominent fluorescence enhancement observed upon mixing HNAPP and Zn^{2+} remained unchanged, even in the presence of a 10-fold excess of metal ions such as K^+, Na^+, and Ca^{2+} (Fig. 5, purple bar).

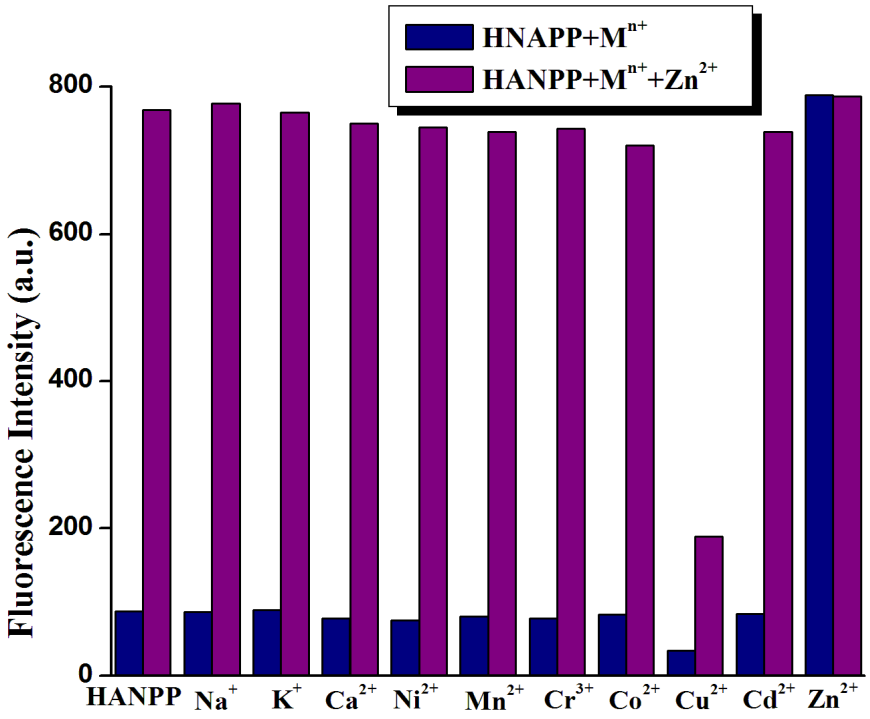

Fig. 5 Metal-ion sensitivity of HNAPP in presence of different metals. Blue bars represent the fluorescence sensitivity of HNAPP (2 x 10^{-5} M) to various metal ions. Purple bars represent the fluorescence response measured after the addition of Zn^{2+} (1 x 10^{-5} M) to the indicated metal ion–complex **1** (1:1 for transition metal ions and 10:1 for alkali and alkaline earth metal ions) in 10 mM HEPES aqueous buffer–CH_3OH (3 : 2, v/v) following excitation at 390 nm (slit width 5 nm).

This confirms the excellent selectivity of HNAPP for Zn^{2+} over other abundant cations. Notably, the fluorescence intensity of the zinc complex was partially quenched in the presence of metal ions such as Mn^{2+}, Cr^{3+}, Ni^{2+}, Cd^{2+} and Co^{2+}. It is interesting to note that the fluorescence intensity of HNAPP in the presence of Zn^{2+} is significantly quenched by Cu^{2+}metal ion probably due to strong binding affinity towards the ligand.

Titration of HNAPP with quencher

An exceptional case appeared that the fluorescence intensity of HNAPP in the presence of Zn^{2+} is slightly quenched by Cu^{2+} metal ion probably due to strong binding affinity towards the probe. As shown in Fig. 6a shows the fluorescence spectra of HNAPP in presence of different concentrations of Cu^{2+} excited at 400 nm in aqueous buffer–CH_3OH (2 : 1, v/v) at pH 7.2. It was seen that the ligand showed one intense peaks at 485 nm during excitation at 400 nm with larger slit width and the fluorescence intensity gradually decreases in presence of Cu^{2+}. It is observed that there is no change in the intensity at 485 nm after the addition of excess of 1.0 equivalent of Cu^{2+} ion with respect to 2.0 equivalent of HNAPP (Fig. 6c).

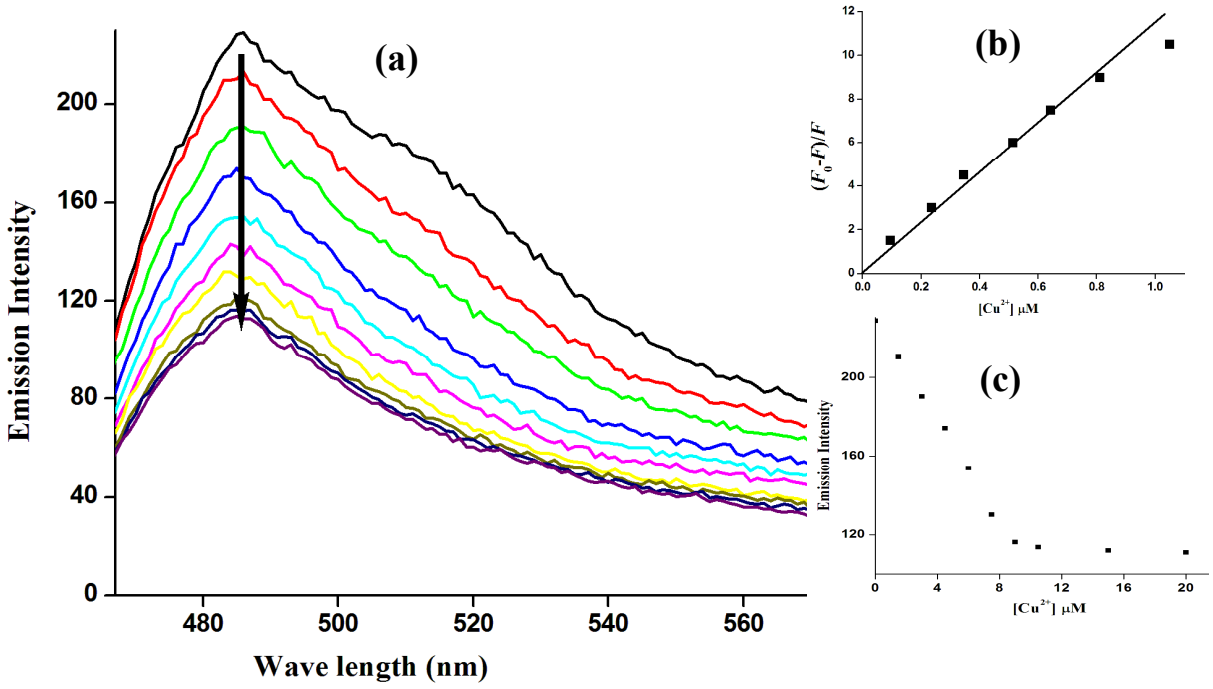

Fig. 6 (a) Fluorescence titration of HNAPP (20 µM) with gradual addition of Cu^{2+} (0-12 µM) in aqueous buffer–CH_3OH (3 : 2, v/v) at pH 7.2; (b) A plot of (*Fo* – *F*)/*F* against [Cu^{2+}] for

HNAPP. Binding constant, K (± 5 %), value determined from the slope of the plot as 11.68 x 10^6 M^{-1}; (c) Emission Intensity at 485 nm vs. [Cu^{2+}]; [slit width (Ex/Em: 10/10)].

This result corroborated with the formation of 1:2 (M:L) complex in solution. This change in fluorescence intensity at 485 nm is used to estimate *K* for the binding of Cu^{2+} to HNAPP by eq 4.[24ab]

$$\log(F_0 - F)/F = \log K + n\log[M^{n+}] \text{.....4}$$

Here F_o and F are the fluorescence intensity of the probe, at 485 nm in the absence and the presence of different concentrations of Cu^{2+} respectively. The inset of Fig. 6b shows a linear plot passing through the origin for $(Fo - F)/F$ vs [Cu^{2+}] (n=1). From this, according to eq 4, the value of *K* was estimated 11.68 x 10^6 M^{-1} respectively, for Cu^{2+} towards HNAPP. The reaction of Cu^{2+} with the chelating agent HNAPP induced rigidity in the resulting molecule and produced a large CHEQ effect which further induced to decrease the fluorescence intensity.

Titration of HNAPP with Zn(II)

In the fluorescence titration experiment, receptor was subjected to excitation at 405 nm and was monitored after each stepwise addition of Zn^{2+} ion to the solution in aqueous buffer–CH_3OH (3 : 2, v/v) at pH 7.2 (Fig. 7). The probe showed comparable weak emitter with respect to complex probably because of quenching by the occurrence of a photo induced electron transfer (PET) process due to the presence of a lone pair of electrons of the donor atoms in the ligand (*N*, *O* donor). A gradual enhancement (~ 12 fold) of the fluorescence intensity was observed at 492 nm upon increasing the concentration of Zn^{2+} ions (Fig. 7a). The reaction of Zn^{2+} with the chelating agent HNAPP induced rigidity in the resulting molecule, reduced the PET mechanism and produced a large CHEF effect which tends to produce a strong 'switch on' blue fluorescence. Inset of Fig. 7c describes a plot of emission intensity at 492 nm against the titration of Zn^{2+} from 0 to 1.2 equivalents. It is clear from the plot that the fluorescence intensity reaches a plateau after addition of exactly 1.0 equivalent of Zn^{2+} ions and there is no significant enhancement of the fluorescence intensity on further addition of Zn^{2+}. This result strongly corroborates with the formation of 1:2 (M:L) complex.

The binding constant values have been determined from the emission intensity data[24c] using the Benesi-Hildebrand equation: $1 / \Delta F = 1 / \Delta F_{max} + (1 / K[C])(1 / \Delta F_{max})$ to establish the

binding abilities of the probe with Zn^{2+}. Here, $\Delta F = Fx - F_0$ and $\Delta F_{max} = F_\infty - F_0$, where F_0, F_x and F_∞ are the emission intensities of the probe used in the absence of Zn^{2+}, at an intermediate Zn^{2+} concentration, and at a concentration of complete interaction, respectively, and where K is the binding constant and [C] the Zn^{2+} concentration. As shown in Fig. 7b the intercept value 1.05 ± 0.5, close to 1.0, also manifests the self-consistency of the experimental data. Therefore, the ligand association constant K is reciprocal of slope, 5.2 x 10^4 M^{-1}. The 1: 2 complex formation in solution is further confirmed by ESI-MS^+-(m/z) analysis (see experimental section).

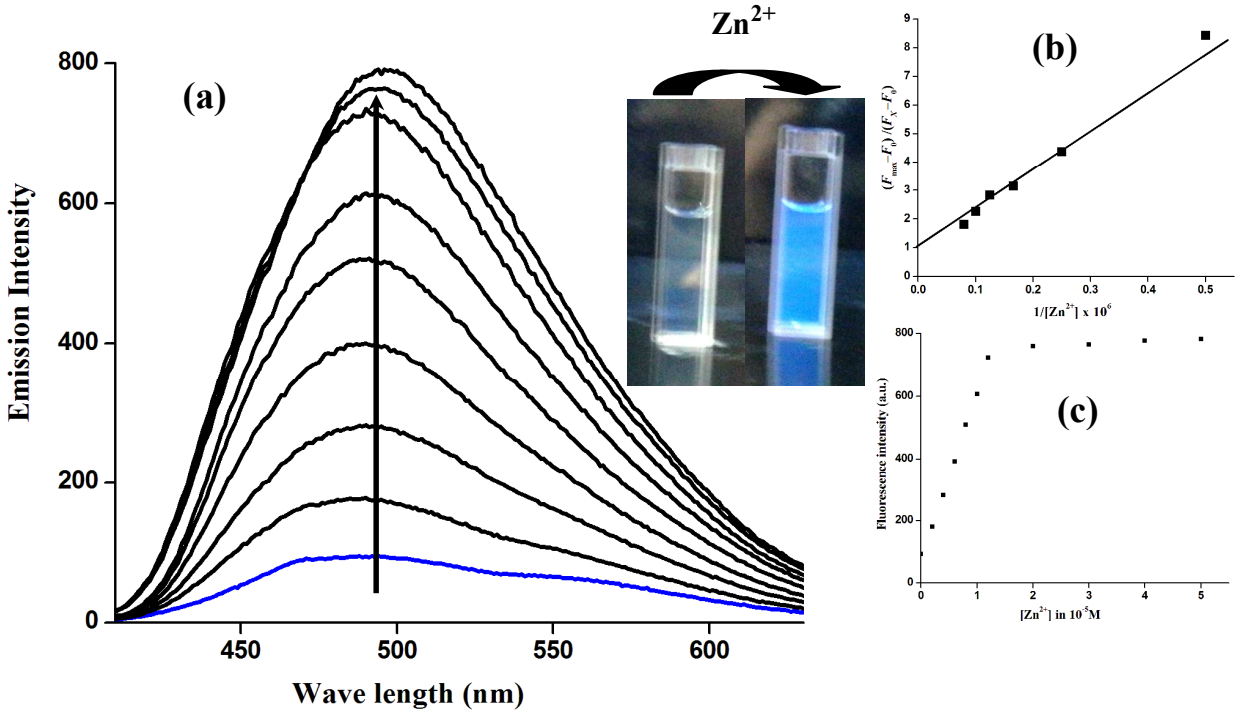

Fig. 7 (a) Fluorescence titration of HNAPP (20 μM) with gradual addition of Zn^{2+} (0-12 μM) in aqueous buffer–CH_3OH (3 : 2, v/v) at pH 7.2; (b) A plot of $(F_\infty - F_0)/(F_x - F_0)$ against 1/[C] for HNAPP. Binding constant, K (± 5 %), value determined from the reciprocal of the slope of the plot as 5.2 x 10^4 M^{-1}; (c) Emission Intensity at 492 nm vs. $[Zn^{2+}]$.

Effect of pH

In addition to metal ion selectivity, for many biological applications, it is very important that the probe can be suitable for measuring specific cation and anion in the physiological pH range. Therefore, I measured the fluorescence intensity of HNAPP in the absence and presence of Zn^{2+} at various pH values. As shown in Fig. 8, the emission intensity of HNAPP slightly

increases gradually at first and then decreases in acid conditions with maximal fluorescence occurring at pH ~5.0. And essentially no change can be observed under neutral and alkaline conditions (pH 7-13). However, the Zn^{2+} -induced fluorescence enhancement of HNAPP continues increasing in the pH 1.2-6.5 range, which may be due to the competition of H^{+}.[25] The emission of [Zn-$NAPP_2$] maintains fairly intense from pH ~7 to pH ~8.7 and is ~70% quenched at higher pH (~13). The observed decreasing response at pH >9.5 may be due to the formation of $Zn(OH)^{+}$ or $Zn(OH)_2$ and thus reducing the concentration of [Zn-$NAPP_2$]. However, HNAPP exhibits satisfactory Zn^{2+} sensing abilities when the pH is in the range of 6.5-8.5, indicating that HNAPP possesses the highest sensing ability in an environment similar to serum (pH ca. 7.3).

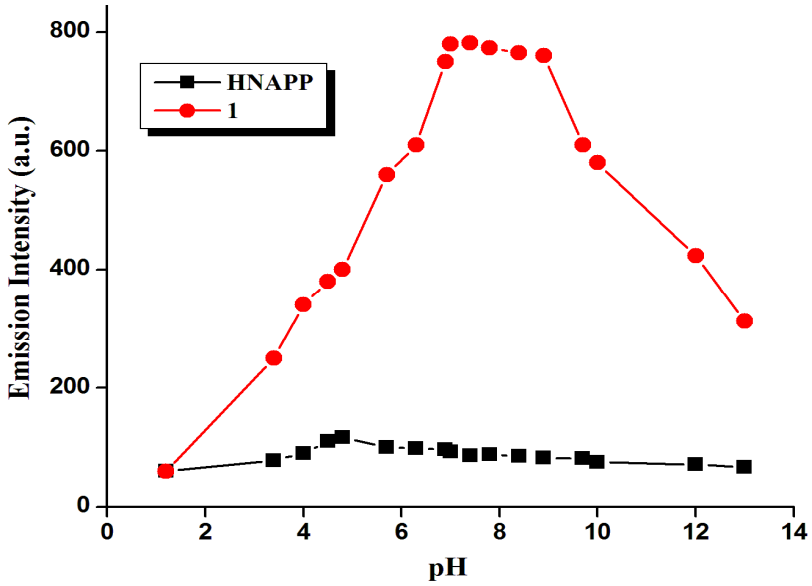

Fig. 8 Fluorescence intensities of HNAPP and Zn-$NAPP_2$ at various pH values at room temperature, CH_3CN-H_2O (1:4, v/v), λ_{ex}=400 nm. A starting solution (CH_3CN-H_2O) of 100 mM NaOH and 10 mM NaCl (pH~13) was used for pH titrations. The pH values were lowered to ~1.3 by the addition of aqueous HCl (CH_3CN-H_2O).

Life time measurement

Time resolved luminescence spectra proved to be an important tool to understand the decay process and the emissive nature of the complex. Thus time resolved luminescence spectra were recorded for both the ligand and the complex in DCM solvent at room temperature using 370 nm excitation. The ligand shows mono exponential while the complex a biexponential decay

nature was given in Fig. 9. The average life time τ_f, ($\tau_f = \alpha_1\tau_1 + \alpha_2\tau_2$, where α_1 and α_2 are relative amplitudes of decay process) has been used to compare excited state stability of the ligand and the complex and the values are 0.5 ns for HNAPP whereas around 7 ns for the complex. The value of τ_1 life time of the complex was of similar order with the lifetime of corresponding ligand which revealed that in excited state the biexponential decay nature of the complex arise due to the contribution of the ligand moiety and the complex itself. The radiative and non radiative rate constant for the ligand and complex are evaluated in Table 3. The non-radiative decay rate constant is much higher than the radiative decay rate constant for the ligand making it weak emitters. On the other hand during complexation the smaller k_{nr} value (ten times lesser) for the complex compared to that of the isolated ligand suggested the enhancement of fluorescence intensity.

Table 3 Photophysical parameters of the ligand and complex in DCM at room temperature.

	Φ_F	k_r, s^{-1} ($\times 10^9$)	k_{nr}, s^{-1} ($\times 10^9$)	τ_1, ns	τ_2, ns	τ_{av}, ns	X^2
HNAPP	0.051	0.102	1.89	0.5	-	0.5	0.97
Zn-NAPP$_2$	0.45	0. 064	0.07	2.7	16.1	7	1.06

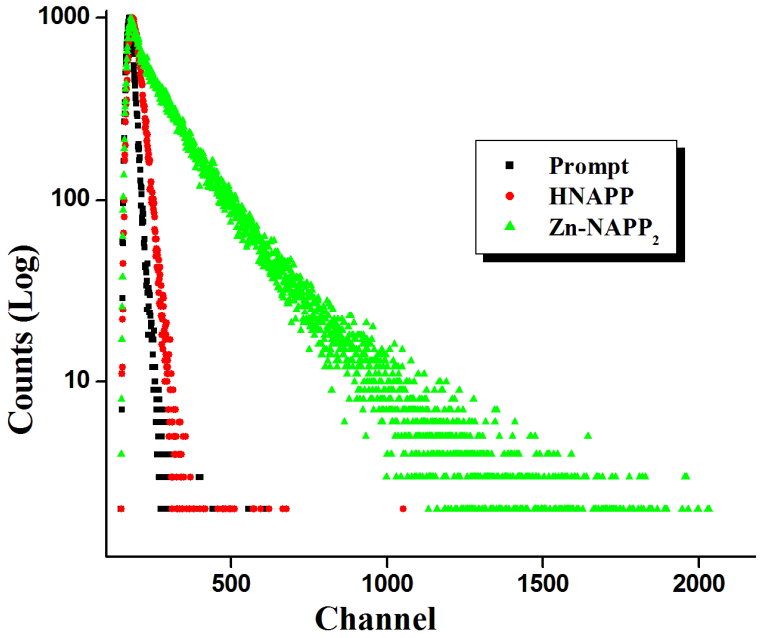

Fig. 9 Changes in the time-resolved photoluminescence decay of HNAPP and Zn-NAPP$_2$ in DCM at room temperature obtained with 370 nm excitation.

Anion selectivity of the complex

To evaluate whether the Zn-NAPP$_2$ complex could be used as an anion-selective fluorescent system, the response of the Zn-NAPP$_2$ complex toward physiologically and environmentally important anions was given in Fig. 10a. Here di hydrogen phosphate (H_2P) and mono hydrogen phosphate (HP) are abbreviated as inorganic hydrogen phosphate (pi). A turn-off fluorescence response was observed for the emission band with a maximum at 492 nm in the presence of externally added solution of Pi at pH 7.2 (Fig. 10b). Interestingly other anions and nucleotides like F^-, Cl^-, Br^-, I^-, AcO^-, PPi, CN^-, ATP, ADP and AMP do not react with Zn-NAPP$_2$ and are thus unable to extrude the zinc ion from the complex. The Zn-NAPP$_2$ system revealed a remarkably selective fluorescence quenching behavior only in presence of Pi ion even at present of similar type pyrophosphate (PPi) anion the receptor Zn-NAPP$_2$ remain silent. Hence my probe simultaneously detected two phosphate anions at physiological pH.

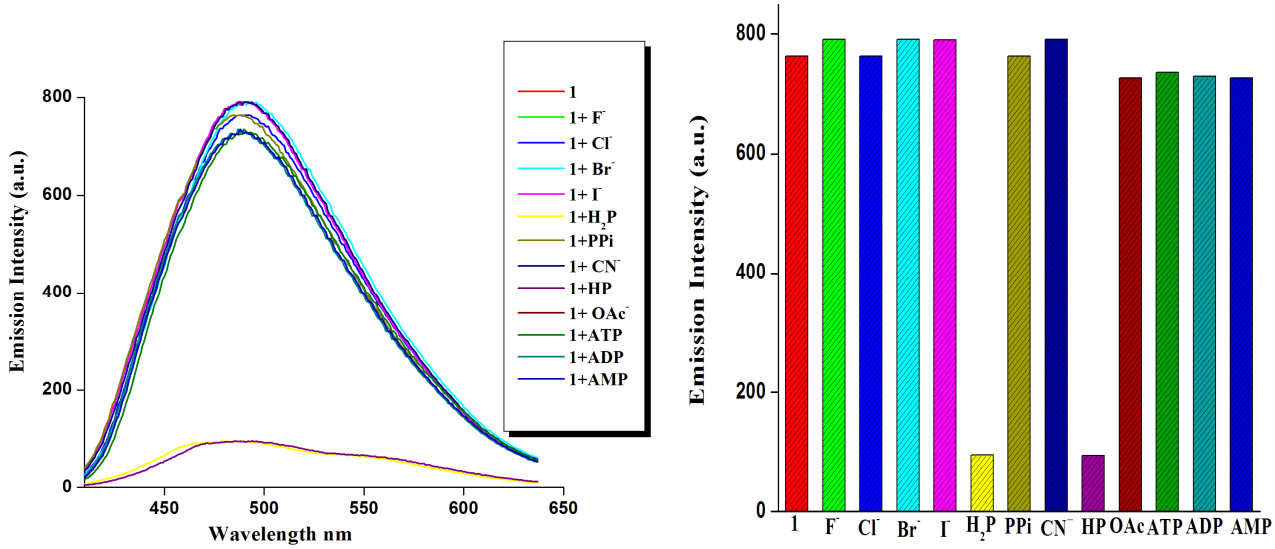

Fig. 10 (a) Emission spectra spectra of **1**(10 μM) with different anions in 3:2 v/v MeOH/water in HEPES buffer at pH 7.2 in the presence of different anion ions (10 μM) at room temperature; (b) Histogram of anion selectivity for complex **1**. λ_{ex} = 400 nm.

The interesting feature is that at this pH both the phosphate anions are undergoes in equilibrium. The equilibrium constant of the reaction H_2P (aq) ↔ H^+ (aq) + HP (aq) is K_a = 6.2 x

10^{-8} which indicates that at this physiological pH both the form of inorganic phosphate are present in almost equal concentration. To gain further insight into the sensing property of phosphate anions, I carried out the titration of phosphate anions separately against the receptor (Zn-$NAPP_2$) at different pH. The buffers used were MES (pH 6.0–6.5), and TRIS (pH 9.0–9.5). It was observed from the Figs. 10 and 11, that in lower pH medium the complex shows slightly lower emission intensity before the addition of inorganic phosphate. This is may be due to the rate of deprotonation of the ligand (HNAPP) is quite smaller i. e. lower complexation ability diminishes the emission intensity in acidic medium. The titration of H_2P against Zn-$NAPP_2$ was carried out ah lower pH at 6.5 while the other titration take place at higher pH (9.0). In acidic medium the above equilibrium shifted towards left side; hence the percentage of H_2P is much more than the HP whereas at higher pH medium HP is predominant. Both the ratio metric titrations of the complex against the Pi are given in Fig.11. As shown in Fig. 11a, there were unique changes in emission intensity of the complex upon addition of H_2P anion. The interesting observation was that there is no further decreasing in fluorescence intensity at 490 nm was observed after the addition of excess of ~2.1 equivalent of H_2P anion with respect to 1.0 equivalent of fluorophore Zn-$NAPP_2$. The mol ratio plot for the binding between Zn^{2+} and H_2P anion corresponds to 1:2 stoichiometries.

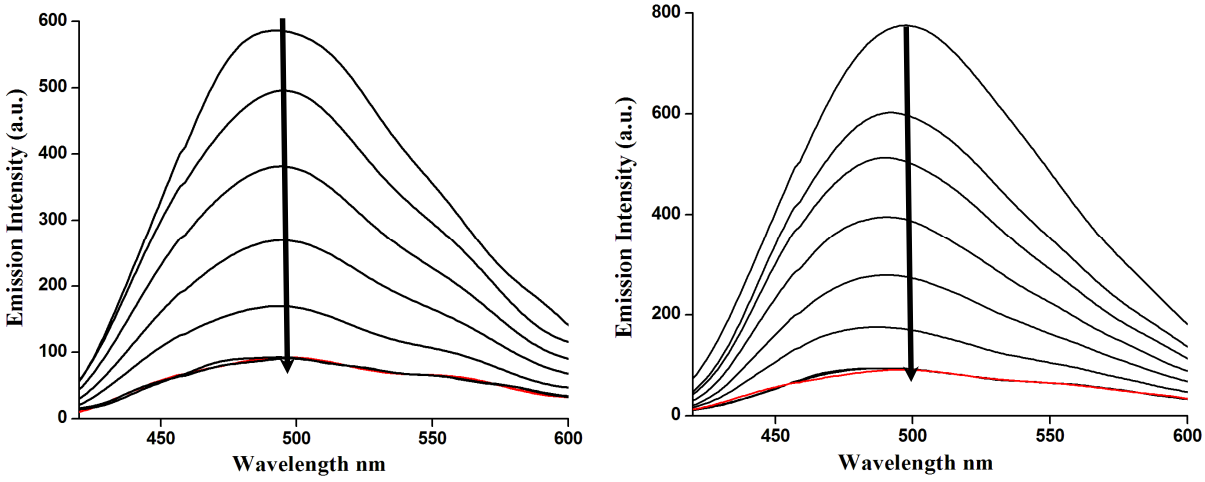

Fig. 11 (a) Fluorescence spectra of Zn-$NAPP_2$ (10 μM) in 3:2 v/v MeOH/water in MES buffer at pH 6.5, upon progressive addition of H_2P anion at room temperature; (b) Fluorescence spectra of Zn-$NAPP_2$ (10 μM) in 3:2 v/v MeOH/water in TRIS buffer at pH 9.0, upon progressive addition of HP anion at room temperature; λ_{ex} = 400 nm

On the other hand the ratio metric titration for HP with the fluorophore at higher pH medium given the similar quencher behavior but the difference arises in mol ratio plot (Fig. 12). In this case the emission intensity decreases until ~1.2 equivalent of HP added with respect to the 1.0 equivalent of fluorophore. The mol ratio plot for the binding between Zn^{2+} and HP anion corresponds to 1:1 stoichiometry. Thus, the experimental results indicate that in both cases the Zn-$NAPP_2$ complex was demetallation and HNAPP was released, which was ascribed due to the formation of an inorganic complex between Zn^{2+} and the Pi anions[26] while there was no interaction between HNAPP and these anions.[27] Moreover, the presence of other investigated anions do not interfere towards these anion sensitivity of Zn-$NAPP_2$ complex, even when the concentrations of these anions were increased to 20-fold compared to that of the investigated anions. These results show that the Zn-$NAPP_2$ system have a high selectivity and sensitivity towards Pi anions.

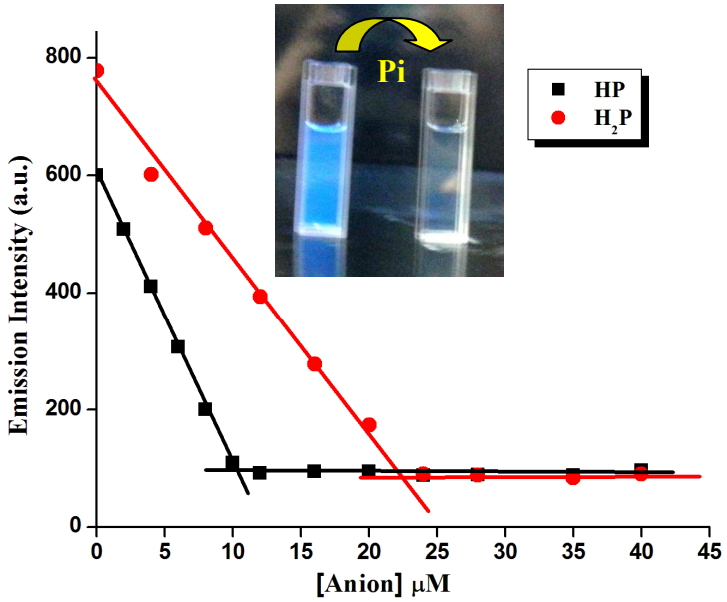

Fig. 12 Fluorescence intensity of **1** *vs* different concentration of HP and H_2P anions (Pi) at different pH.

Logic gate

Based on the above observations, I investigated the different fluorescence state ‘‘ON and OFF’’ of HNAPP with changing the addition sequence for finding out some interesting

chemistry related to mimicking advanced logic operations. The enhancement of fluorescence by zinc ions and the quenching of the fluorescence by Pi at physiological pH can be usefully employed in the construction of a logic gate. To evaluate the exact phenomenon the reversibility test has been performed in which Zn^{2+} ions and Pi were added to HNAPP in an alternate and reversible fashion. In the presence of Zn^{2+} ions the fluorescence of HNAPP is enhanced, and on the addition of Pi to the solution of receptor (Zn-$NAPP_2$) the enhanced fluorescence gradually decreases and again on further addition of Zn^{2+} to the mixture the fluorescence intensity once again increases. This type of behavior is like mimicking the **INHIBIT** logic gate at λ_{max} = 400 nm. A basic two-input **INHIBIT** can be obtained for HNAPP ($c = 2 \times 10^{-5}$ M) with the action of Zn^{2+} ($c = 2 \times 10^{-4}$ M) and Pi anion ($c = 2 \times 10^{-4}$ M) as inputs.[28] For the input, the fluorescence emission enhancement at 492 nm of HNAPP in the presence of Zn^{2+} and in the absence of Pi is defined as the "**1**" state and in the other circumstances the quenching of the fluorescence of HNAPP is defined as the "**0**" state. Zn^{2+} in this case should lead to fluorescence enhancement in its occupied state (at 492 nm) in the absence of Pi, equivalent to a **YES** operation (input **1**). The interaction of the other input, i.e. Pi in this case (input **2**), with its corresponding receptor should lead to fluorescence quenching, thereby implementing the necessary **NOT** gate. The receptor, i.e. HNAPP (occupied or free), acts in parallel on the fluorescence output signal, which implement the required **AND** function. In the presence of both inputs, the quenching (by input **2**) should override the fluorescence enhancement by input **1**, in accordance with the truth table and the circuit for the **INHIBIT** gate as shown in Fig. 13.

(a)

INPUT		OUTPUT
Zn^{2+}	Pi	INH(FL)
0	0	0
1	0	1
0	1	0
1	1	0

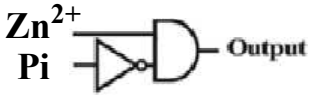

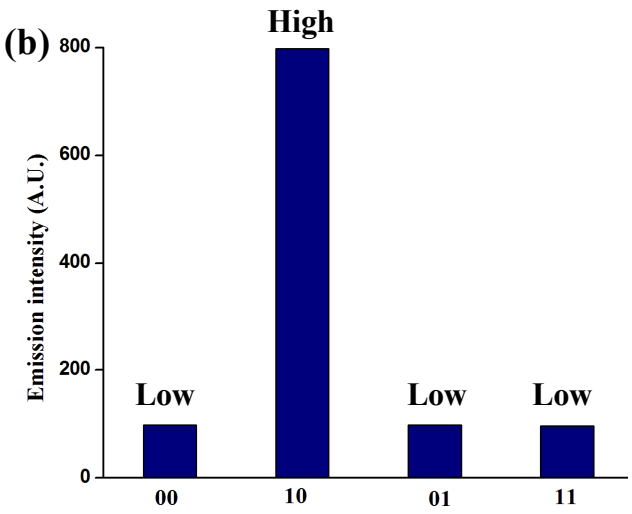

Fig. 13 (a) The logic table of the INHIBIT gate with the circuit. (b) Fluorescence output of HNAPP (c = 2 × 10^{-5} M) (λ_{ex} = 400 nm) in the presence of chemical inputs, Zn^{2+} (c = 2 × 10^{-4} M) and Pi (c =2 × 10^{-4} M) in 3:2 v/v MeOH/water in HEPES buffer at pH 7.2.

Conclusions

So as a whole, I have developed a turn-on fluorescent chemo probe based on a naphthaldehyde-aminophenol conjugate. The probe display an excellent selectivity and high sensitivity toward the detection of Zn^{2+} in 10 mM HEPES aqueous buffer–CH_3OH (3 : 2, v/v) over a wide range of tested metal ions remarkably by fluorescence method. The emission of the ligand appeared due to excited state intramolecular proton transfer, ESIPT whereas the high emissive complex shows emission property for chelation-enhanced fluorescence (CHEF) process. The detection limit of HNAPP for Zn^{2+} (10 μM) was below the guidelines of the WHO (76 μM). The DFT calculation reveals that ICT process take place from the naphthyl ring (donor, HOMO) to azo methine moiety (acceptor, LUMO). In addition, the addition of HP/H_2P at physiological pH quenches the fluorescence of receptor Zn-$NAPP_2$ complex indicating that HNAPP is a reversible chemosensor. The metal-anion induced 'Off–On–Off' type fluorescence response as a probe has been carefully employed to function as a molecular switch.

Acknowledgements

The valuable discussion with Dr. Kajal Krishna Rajak, is kindly acknowledged. Author thanks the UGC of India for financial support and Jadavpur University for instrumental facilities.

Notes

Department of Chemistry, Jadavpur University, Kolkata 700032, India. E-mail: amarjuchem@gmail.com

† Electronic Supplementary Information (ESI) available: Figs. S1-S6†.

References

1 (a) A. P. De Silva, H. Q. N. Gunaratne, T. Gunnlaugsson, A. J. M. Huxley, C. P. McCoy, J. T. Rademacher and T. E. Rice, *Chem. Rev.,* 1997, **97**, 1515-1566; (b) L. Prodi, F. Bolletta, M. Montalti and N. Zaccheroni, *Coord. Chem. Rev.,* 2000, **205**, 59-83; (c) A. Hens, A. Maity and K. K. Rajak .*Inorg. Chimica Acta.,* 2014**, 423**, 408–420; (d) H. N. Kim, M. H. Lee, H. J. Kim, J. S. Kim and J. Yoon, *Chem. Soc. Rev.,* 2008, **37**, 1465-1472; (e) A. Hens and K. K. Rajak *RSC Adv.,* DOI: 10.1039/C5RA05145B.

2 (a) B. Valeur and I. Leray, *Coord. Chem. Rev.,* 2000, **205**, 3-40; (b) K. Rurack and U. Resch-Genger, *Chem. Soc. Rev.,* 2002, **31**, 116-127; (c) V. Amendola, L. Fabbrizzi, F. Forti, M. Licchelli, C. Mangano, P. Pallavicini, A. Poggi, D. Sacchi and A. Taglieti, *Coord. Chem. Rev.,* 2006, **250**, 273-299; (d) L. Prodi, F. Bolletta, M. Montalti and N. Zaccheroni, *Coord. Chem. Rev.,* 2000, **205**, 59-83; (c) J. S. Kim and D. T. Quang, *Chem. Rev.,* 2007, **107**, 3780-3799; (d) H. N. Kim, M. H. Lee, H. J. Kim, J. S. Kim and J. Yoon, *Chem. Soc. Rev.,* 2008, **37**, 1465-1472.

3 (a) T. V. O'Halloran, *Science,* 1993, **261**, 715-725; (b) J. Y. Koh, S. W. Suh, B. J. Gwag, Y. Y. He, C. Y. Hsu and D. W. Choi, *Science,* 1996, **272**, 1013-1016; (c) F. Walker and R. E. Black, *Annu. Rev. Nutr.,* 2004, **24**, 255-275; (d) C. J. Frederickson and A. I. Bush, *Biometals,* 2001, **14**, 353-366.

4 (a) E. M. Nolan, J. Jaworski, K.-I. Okamoto, Y. Hayashi, M. Sheng and S. J. Lippard, *J. Am. Chem. Soc.,* 2005, **127**, 16812-16823; (b) E. M. Nolan, S. C. Burdette, J. H. Harvey, S. A. Hilderbrand and S.J. Lippard, *Inorg. Chem.,* 2004, **43**, 2624-2635; (c) T. Koike, T. Abe, M. Takahashi, K. Ohtani, E. Kimura and M. Shiro, *J. Chem. Soc., Dalton Trans.,* 2002, 1764-1768; (d) S. C. Burdette, G. K. Walkup, B. Spingler, R. Y. Tsien and S. J. Lippard, *J. Am. Chem. Soc.,* 2001, **123**, 7831-7841.

5 (a) T. Harano, K. Kikuchi, Y. Urano and T. Nagano, *J. Am. Chem. Soc.*, 2002, **124**, 6555-6562: (b) S. C. Burdette and S. J. Lippard, *Coord. Chem. Rev.*, 2001, **216**, 333-361; (c) A. Hens, P. Mondal, and K. K. Rajak *Dalton Trans*. 2013, 42, 14905- 14915; (d) M. D. Shultz, D. A. Pearce and B. Imperiali, *J. Am. Chem. Soc.*, 2003, **125**, 10591-10597; (e) A. Hens and K. K. Rajak RSC Adv., 2015, 5, 4219-4232.

6 (a) E. T. Elsaesser, H. J. Bakker, H. J. *Ultrafast Hydrogen Bonding Dynamics and ProtonTransfer Processes in the Condensed Phase*, Kluwer, Dordrecht, 2002. (b) X. Zhou, B. Yu, Y. Guo, X. Tang, H. Zhang and W. Liu, *Inorg. Chem.*, 2010, **49**, 4002-4007; (c) B. Zhang, K. Cao and X. Zeng, *Eur. J. Inorg Chem.*, 2012, 3844-3851; (d) M. Irie, *Chem. Rev.*, 2000, **100**, 1683-1684; (e) R. Pandey, P. Kumar, A. K. Singh, M. Shahid, P. Li, S. K. Singh, Q. Xu, A. Misra and D. S. Pandey, *Inorg. Chem*., 2011, **50**, 3189-3197; (f) S. A. Ingale and F. Seela, *J. Org. Chem.*, 2012, **77**, 9352-9356; (g) S. M. Aldoschin, L. O. Atovmian, *Problemy Kristalokhimii*, Poraj-Koshic, M. Eds., Nauka, Moscow, 1984.

7 (a) M. N. Manjunatha, A. G. Dikundwar and K. R. Nagasundara, *Polyhedron,* 2011, **30,** 1299-1304; (b) E. M. Nolan, and S. J. Lippard, *Inorg. Chem.,* 2004, **43**, 8310–8317; (c) E. M. Nolan, S. C. Burdette, J. H. Hervey, S. A. Hilderbrand and S. J. Lippard, *Inorg. Chem.*, 2004, **43**, 2624–2635; (d) S. Aoki, D. Kagata, M. Shiro, K. Takeda and E. Kimura, *J. Am. Chem. Soc.*, 2004, **126**, 13377–13390; (e) N. C. Lim, J. V. Schuster, M. C. Porto, M. A. Tanudra, L. Yao, H. C. Freake and C. Breuckner, *Inorg. Chem.,* 2005, **44**, 2018–2030; (f) R. Parkesh, T. C. Lee and T. Gunnlaugsson, *Org. Biomol. Chem.*, 2007, **5**, 310–317; (g) S. Ray, S. Konar, A. Jana, S. Jana, A. Patra, S. Chatterjee, J. A. Golen, A. L. Rheingild, S. S. Mondal and S. K. Kar, *Polyhedron,*2012, **33**, 82-89; (h)

8 (a) I. B. Mahadevan, M. C. Kimber, S. F. Lincoln, E. R. Tiekink, A. D. Ward, W. H. Betts, I. J. Forbes and P. D. Zalewski, *Aust. J. Chem.* 1996, **49**, 561-568; (b) P. D. Zalewski, I. J. Forbes and W. H. Betts, *Biochem. J.* 1993, **296**, 403-408; (c) C. J. Frederickson, E. J. Kasarskis, D. Ringo and R. E. Frederickson, *J. Neurosci. Methods* 1987, **20**, 91-103; (d) C. J. Frederickson, *J. Int. Rev. Neurobiol.* 1989, **31**, 145-238; (e) S. A. Ingale and F. Seela, *J. Org. Chem.,* 2012, **77**, 9352−9356.

9 (a) W. Scenger, *Principles of Nucleic AcidStructure*, Springer, New York, 1998; (b) D. H. Lee, S. Y. Kim and J. Hong, *Angew. Chem., Int. Ed.*, 2004, **43**, 4777–4780.

10 (a) M. Doherty, C. Becher, M. Regan, A. Jones and J. Ledingham, *Ann. Rheum. Dis.,* 1996, **55**, 432-436; (b) A. Hens, P. Mondal and K. K. Rajak *Polyhedron,* 2015, **85**, 255–266.

11 W. H. Melhuish, *J. Phys. Chem.*, 1961, **65**, 229-235.

12 (a) P. Mondal, A. Hens, S. Basak and K. K. Rajak, *Dalton Trans.*, 2013, **42**, 1536-1549; (b) B. Valuer, *Molecular Fluorescence*: *Principle and Applications*, Wiley-BCH, Weinbeim, 2001.

13 (a) K. Wolinski, J. F. Hinton and P. Pulay, *J. Am. Chem. Soc.*, 1990, **112**, 8251-8260; (b) P. Taehtinen, A. Bagno, K. Klika and K. Pihlaja, *J. Am. Chem. Soc.*, 2003, **125**, 4609-4618; (c) F. Cloran, I. Carmichael and A. S. Serianni, *J. Am. Chem. Soc.*, 2001, **123**, 4781-4791.

14 E. Runge and E. K.U. Gross, *Phys. Rev. Lett.*, 1984, **52**, 997-1000.

15 (a) M. E. Casida, C. Jamoroski, K. C. Casida and D. R. Salahub, *J. Chem. Phys.*, 1998, **108**, 4439-4449; (b) R. E. Stratmann, G. E. Scuseria and M. J. Frisch, *J. Chem. Phys.*, 1998, **109**, 8218-8224; (c) R. Bauernschmitt and R. Ahlrichs, *Chem. Phys. Lett.*, 1996, **256**, 454-464.

16 (a) A. D. Becke, *J. Chem. Phys.*, 1993, **98**, 5648-5652; (b) C. Lee, W. Yang and R. G. Parr, *Phys. Rev. B*, 1988, **37**, 785-789.

17 (a) M. Cossi, N. Rega, G. Scalmani and V. Barone, *J. Comput. Chem.*, 2003, **24**, 669-681; (b) M. Cossi and V. Barone, *J. Chem. Phys.*, 2001, **115,** 4708-4717; (c) V. Barone and M. Cossi, *J. Phys. Chem. A*, 1998, **102**, 1995-2001.

18 (a) A. Douhal, F. Lahmani and A. Zewail, *Chem. Phys.*, 1996, **207**, 477-498 ; (b) J. Catalan and J. L. P. de Paz, *J. Phys. Chem. A*, 2001, **105**, 7315-7316.

19 M. J. Frisch, G. W. Trucks, H. B. Schlegel, G. E. Scuseria, M. A. Robb, J. R. Cheeseman, G. Scalmani, V. Barone, B. Mennucci, G. A. Petersson, H. Nakatsuji, M. Caricato, X. Li, H. P. Hratchian, A. F. Izmaylov, J. Bloino, G. Zheng, J. L. Sonnenberg, M. Hada, M. Ehara, K. Toyota, R. Fukuda, J. Hasegawa, M. Ishida, T. Nakajima, Y. Honda, O. Kitao, H. Nakai, T. Vreven, J. A. Montgomery Jr., J. E. Peralta, F. Ogliaro, M. Bearpark, J. J. Heyd, E. Brothers, K. N. Kudin, V. N. Staroverov, R. Kobayashi, J. Normand, K.

Raghavachari, A. Rendell, J. C. Burant, S. S. Iyengar, J. Tomasi, M. Cossi, N. Rega, J. M. Millam, M. Klene, J. E. Knox, J. B. Cross, V. Bakken, C. Adamo, J. Jaramillo, R. Gomperts, R. E. Stratmann, O. Yazyev, A. J. Austin, R. Cammi, C. Pomelli, J. W. Ochterski, R. L. Martin, K. Morokuma, V. G. Zakrzewski, G. A. Voth, P. Salvador, J. J. Dannenberg, S. Dapprich, A. D. Daniels, Ö. Farkas, J. B. Foresman, J. V. Ortiz, J. Cioslowski and D. J. Fox, *Gaussian 09*, *(Revision A.1)*, Gaussian, Inc., Wallingford, CT, 2009.

20 N. M. O'Boyle, A. L. Tenderholt and K. M. Langner, *J. Comp. Chem.*, 2008, **29**, 839-845.

21 (a) K. Wolniski, J. F. Hilton and P. Pulay, *J. Am. Chem. Soc.*, 1990, **112**, 8251-8260; (b) R. Ditchfield, *Mol. Phys.*, 1974, **27**, 789-807; (c) R. Mcweeny, *Phys. Rev.*, 1962, **126**, 1028-1034; (d) F. London, *J. Phys. Chem.*, 1937, 397-409.

22 C. M. Rohlfing, L. C. Allen and R. Ditchfield, *Chem. Phys.*, 1984, **87**, 9-15.

23 (a) M. Cossi, V. Barone, B. Mennucci and J. Tomasi, *Chem. Phys. Lett.*, 1998, **286**, 253-260; (b) E. Cancès, B. Mennucci and J. Tomasi, *J. Chem. Phys.*, 1997, **107**, 3032-3041; (c) Z. Li, W. Zhang, X. Lui, C. Lui, M. Yu and L. Wei, *RSC Adv.,* 2015, **5**, 25229-25235.

24 (a) X. Z. Feng, Z. Lin, L. J. Yang, C. Wang and C. L. Bai, *Talanta* 1998 **47** 12231229; (b) L. Gelamo and M. Tabak *Spectrochim. Acta* 2000 **A56** 2255-2271; (c) H. A. Benesi and J. H. Hildebrand, *J. Am. Chem. Soc.*, 1949, **71**, 2703-2707;

25 (a) P. Roy, K. Dhara, M. Manassero, J. Ratha and P. Banerjee, *Inorg. Chem.* **2007**, 47, 6405-6412; (b) Y. Zhang, X. F. Guo, X. W. Si, L. H. Jia and X. H. Qian, *Org. Lett.* **2008**, 10, 473-476.

26 F. Y. Wu, X. F. Tan, Y. M. Wu and Y. Q. Zhao, *Spectrochim. Acta*, *Part A*, 2006, **65**, 925-929.

27 J. Wang and C. S. Ha, *Tetrahedron*, 2010, **66**, 1846.

28 A. P. de Silva, I. M. H. Dixon, Q. N. Gunaratne, T. Gunnlaugsson, P. R. S. Maxwell and T. E. Rice, J. Am.Chem. Soc., 1999, 121, 1393.